Simple Competition Models for Bem1p-GFP-Snc2p Foci

We imagine that Bem1p-GFP-Snc2p molecules can be in one of four compartments: in one of two foci on the plasma membrane (amounts denoted by h_1 and h_2), in the plasma membrane but not in either focus (amount denoted by h_m), or in an internal pool (amount denoted by h_i). We assume that Bem1p-GFP-Snc2p synthesis and degradation are balanced, so the total amount, H_o, of Bem1p-GFP-Snc2p is conserved, and we have

$$h_1 + h_2 + h_m + h_i \quad = \quad H_o. \tag{1}$$

We assume that Bem1p-GFP-Snc2p is delivered from the internal pool to the two foci via actin cables, with total flux αh_i split between the two foci in a manner proportional to the amounts already in the foci. Bem1p-GFP-Snc2p is removed from both of the foci as well as the general membrane and delivered to the internal pool by endocytosis, at rates proportional to the amounts in the compartments. To accommodate the likelihood (based on actin patch clustering) that endocytosis at foci (γh_1 and γh_2) is more active than endocytosis in the general membrane (δh_m), we use different rate constants. Finally, Bem1p-GFP-Snc2p escapes from the foci to the general membrane compartment by diffusion. Here we are interested in contrasting two different scenarios. Either diffusion-mediated loss is proportional to the amounts h_1 and h_2 (this will be called the proportional model) or it is proportional to $(h_1)^\eta$ and $(h_2)^\eta$ where η is a power satisfying $0 < \eta < 1$ (this will be called the non-proportional model). Biologically, we believe that $0.5 < \eta < 1$.

Physical interpretation of model assumptions. Like previous models of actin-mediated feedback (Wedlich-Soldner et al. 2003; Marco et al. 2007), we treat fluxes of the relevant protein (in our case Bem1p-GFP-Snc2p) in a continuous manner that ignores the vesicular carriers. In reality, of course, the protein is delivered in quantal steps (vesicles) along with additional membrane. We note that by ignoring the quantal nature of vesicle delivery, we fail to account for a significant source of noise (see discussion below). By ignoring the additional membrane, we effectively assume that the protein concentration on exocytic vesicles is higher than it is at any point on the plasma membrane (consider that if this were not the case, then fusion of the exocytic vesicle near the polarization site would dilute, rather than concentrate, the protein at the site of fusion, and the positive feedback reinforcement would not work). We believe that this assumption is justified because v-SNAREs like Snc2p are indeed highly concentrated (and exert their function) on exocytic vesicles (Protopopov et al. 1993).

We also make the simplifying assumption that the system is at steady state; i.e. that both the total membrane area and the total Bem1p-GFP-Snc2p abundance are constant. Thus, membrane addition (exocytosis) and retrieval (endocytosis) are balanced. We believe that this assumption is justified because the cell size changes only minimally over the relevant timeframe (8 min between polarization and bud emergence). Bem1p-GFP-Snc2p delivery and recycling are also balanced. Because Bem1p-GFP-Snc2p is

highly concentrated on secretory vesicles, this assumption requires that the protein also be highly concentrated on endocytic vesicles, which we believe is justified because Snc2p contains a very effective endocytosis signal (Grote et al. 2000).

Another simplifying assumption is that in cells that have developed two strong foci, all delivery of Bem1p-GFP-Snc2p from internal stores is directed to one or other focus. This is equivalent to assuming that all actin cables are captured by one or the other focus, despite the expectation that a considerable amount of Bem1p-GFP-Snc2p is distributed throughout the general membrane outside the foci. We believe that this assumption is justified because actin staining indicates that a large majority of the detectable cables in unbudded cells terminate at a focus (both in single-focus and two-focus cells: see Fig. 6C). Although cables are faint and often difficult to follow in three dimensions, the myosin V Myo2p and the vesicle marker Sec4p are highly concentrated at the focus in unbudded cells (see, e.g. Pruyne et al. 1998), supporting the idea that vesicle delivery is highly polarized towards foci.

However, we recognize that this assumption is unlikely to accurately represent the early stages of focus growth where many actin cables would be unaligned. Because we do not know the relationship linking Bem1p-GFP-Snc2p concentration to the probability of actin cable capture at these early stages, we only consider the situation once two strong foci have developed. We note that adding a term that allows some delivery of Bem1p-GFP-Snc2p directly from the internal pool (h_i) to the general membrane (h_m) does not affect any of the arguments that follow: it simply adds another parameter that will affect the kinetics but not the outcome of competition between foci.

The assumptions that delivery and endocytosis are proportional to the amount of Bem1p-GFP-Snc2p already present in the focus are admittedly somewhat arbitrary: they are the simplest starting assumptions that can be made without knowing the molecular nature of the many linkages that cause actin cables and patches to polarize.

Analysis of the proportional model. The differential equations of the proportional model are as follows:

$$\frac{dh_1}{dt} = \alpha\frac{h_1(t)}{h_1(t)+h_2(t)}h_i(t) - \beta h_1(t) - \gamma h_1(t) \quad (2)$$

$$\frac{dh_m}{dt} = \beta h_1(t) + \beta h_2(t) - \delta h_m(t) \quad (3)$$

$$\frac{dh_2}{dt} = \alpha\frac{h_2(t)}{h_1(t)+h_2(t)}h_i(t) - \beta h_2(t) - \gamma h_2(t) \quad (4)$$

$$\frac{dh_i}{dt} = \gamma h_1(t) + \gamma h_2(t) + \delta h_m(t) - \alpha h_i(t). \quad (5)$$

Here α, β, γ, and δ are positive constants; their values do not affect the calculations or the conclusions. If $(\overline{h}_1, \overline{h}_2, \overline{h}_m, \overline{h}_i)$ is an equilibrium point, then

$$\beta(\overline{h}_1 + \overline{h}_2) = \delta\overline{h}_m, \quad (6)$$

and

$$\gamma(\overline{h}_1 + \overline{h}_2) + \delta\overline{h}_m \;\; = \;\; \alpha\overline{h}_i, \tag{7}$$

so it follows from (1) that

$$\overline{h}_1 + \overline{h}_2 \;\; = \;\; \frac{H_o}{1 + \frac{\beta}{\delta} + \frac{\gamma+\beta}{\alpha}}. \tag{8}$$

Conversely, if we choose any non-negative $\overline{h}_1$ and $\overline{h}_2$ that satisfy (8) and define $\overline{h}_m$ and $\overline{h}_i$ by (6) and (7), then $(\overline{h}_1, \overline{h}_2, \overline{h}_m, \overline{h}_i)$ is an equilibrium point. Thus, for each H_o, the set of equilibrium points in the positive orthant is the line segment given by (6), (7) and (8).

If we use (1) to substitute for $h_1 + h_2$ in (3) and (5), we find that h_m and h_i satisfy a pair of linear equations:

$$\begin{pmatrix} h_i \\ h_m \end{pmatrix}' \;=\; H_o \begin{pmatrix} \gamma \\ \beta \end{pmatrix} \;-\; A \begin{pmatrix} h_i \\ h_m \end{pmatrix}, \qquad A \;=\; \begin{pmatrix} (\gamma+\alpha) & (\gamma-\delta) \\ \beta & (\beta+\delta) \end{pmatrix}.$$

For all positive choices for the constants $\alpha, \beta, \gamma, \delta$, the eigenvalues of A have strictly positive real parts. Thus given H_o, and any initial conditions, the solutions $h_m(t)$ and $h_i(t)$ converge to $\overline{h}_m = \alpha\beta H_o/\det(A)$ and $\overline{h}_i = \delta(\gamma+\beta)H_o/\det(A)$. By adding equations (2) and (4) we see that $h_1(t) + h_2(t)$ satisfies

$$(h_1(t) + h_2(t))' \;=\; \alpha h_i(t) \;-\; (\gamma+\beta)(h_1(t) + h_2(t)),$$

from which it follows that $h_1(t) + h_2(t)$ converges to the value given by (8) independent of the initial conditions.

Finally, by dividing (2) by (4) we see that $\frac{h_1'}{h_2'} = \frac{h_1}{h_2}$, so

$$\left(\frac{h_1}{h_2}\right)' \;=\; \frac{h_1' h_2 - h_1 h_2'}{h_2^2} \;=\; 0.$$

Thus the ratio $h_1(t)/h_2(t)$ remains constant and the limit point on the line given by (8) is determined by the initial ratio of h_1 and h_2.

We remark that if the total amount of Bem1p-GFP-Snc2p, namely H_o, is kept fixed and noise is added, the system will drift randomly along the line of equilibria given by (8).

Analysis of the non-proportional model. For the non-proportional model the differential equations are

$$\begin{aligned}
\frac{dh_1}{dt} &= \alpha\frac{h_1(t)}{h_1(t)+h_2(t)}h_i(t) - \beta h_1(t)^\eta - \gamma h_1(t) && (9)\\
\frac{dh_m}{dt} &= \beta h_1(t)^\eta + \beta h_2(t)^\eta - \delta h_m(t) && (10)\\
\frac{dh_2}{dt} &= \alpha\frac{h_2(t)}{h_1(t)+h_2(t)}h_i(t) - \beta h_2(t)^\eta - \gamma h_2(t) && (11)\\
\frac{dh_i}{dt} &= \gamma h_1(t) + \gamma h_2(t) + \delta h_m(t) - \alpha h_i(t). && (12)
\end{aligned}$$

where $0 < \eta < 1$. As before, the total amount of Bem1p-GFP-Snc2p is conserved so (1) holds. To investigate equilibria, we set the right hand sides to zero finding:

$$\begin{aligned}
\beta\overline{h}_1^\eta + \beta\overline{h}_2^\eta &= \delta\overline{h}_m && (13)\\
\delta\overline{h}_m + \gamma(\overline{h}_1+\overline{h}_2) &= \alpha\overline{h}_i && (14)\\
(1+\frac{\gamma}{\alpha})(\overline{h}_1+\overline{h}_2) + \beta(\frac{1}{\delta}+\frac{1}{\alpha})(\overline{h}_1^\eta+\overline{h}_2^\eta) &= H_o. && (15)
\end{aligned}$$

Let h_o and h_{oo} denote the two unique positive numbers such that:

$$\begin{aligned}
(1+\frac{\gamma}{\alpha})(2h_o) + \beta(\frac{1}{\delta}+\frac{1}{\alpha})(2h_o^\eta) &= H_o, && (16)\\
(1+\frac{\gamma}{\alpha})(h_{oo}) + \beta(\frac{1}{\delta}+\frac{1}{\alpha})(h_{oo}^\eta) &= H_o. && (17)
\end{aligned}$$

Then, $E = (h_o, h_o, \frac{\beta}{\delta}2h_o^\eta, \frac{\gamma}{\alpha}2h_o + \frac{\beta}{\alpha}2h_o^\eta)$ is an equilibrium with equal amounts of Bem1p-GFP-Snc2p in each spot on the membrane. $(h_{oo}, 0, \frac{\beta}{\delta}h_{oo}^\eta, \frac{\gamma}{\alpha}h_{oo}+\frac{\beta}{\alpha}h_{oo}^\eta)$ and $(0, h_{oo}, \frac{\beta}{\delta}h_{oo}^\eta, \frac{\gamma}{\alpha}h_{oo}+\frac{\beta}{\alpha}h_{oo}^\eta)$ are the unique equilibria with nothing in spot two and nothing in spot one, respectively. To see that E is the only equilibrium with mass in both spot one and in spot two, suppose that $(\overline{h}_1, \overline{h}_2, \overline{h}_m, \overline{h}_i)$ is an equilibrium and $\overline{h}_1 > 0$, $\overline{h}_2 > 0$. At equilibrium,

$$\alpha\frac{\overline{h}_1}{\overline{h}_1+\overline{h}_2}\overline{h}_i - \beta\overline{h}_1^\eta - \gamma\overline{h}_1 = 0. \quad (18)$$

If we solve (13) and (14) for $\overline{h}_i$ in terms of $\overline{h}_1$ and $\overline{h}_2$, substitute in (18), and rearrange, we find that:

$$\beta\overline{h}_1\frac{\overline{h}_1^\eta+\overline{h}_2^\eta}{\overline{h}_1+\overline{h}_2} = \beta\overline{h}_1^\eta, \quad (19)$$

and similarly,

$$\beta\overline{h}_2\frac{\overline{h}_1^{\eta}+\overline{h}_2^{\eta}}{\overline{h}_1+\overline{h}_2} \;=\; \beta\overline{h}_2^{\eta}. \tag{20}$$

From (19) and (20) it follows that $\overline{h}_1^{1-\eta}=\overline{h}_2^{1-\eta}$, so we conclude that $\overline{h}_1=\overline{h}_2$ since $\eta<1$. By (13) and (14), the values of $\overline{h}_1$ and $\overline{h}_2$ determine $\overline{h}_m$ and $\overline{h}_i$, so we have proven that for each total mass, H_o, there is a unique equilibrium, E, in the strictly positive orthant.

We consider the dynamics of $h_1(t)$ and $h_2(t)$ first. Rearranging equations (9) and (11) and then dividing (9) by (11) gives

$$\frac{h_1'+\beta h_1(t)^{\eta}+\gamma h_1(t)}{h_2'+\beta h_2(t)^{\eta}+\gamma h_2(t)} \;=\; \frac{h_1(t)}{h_2(t)},$$

or,

$$h_2(t)h_1'(t)-h_1(t)h_2'(t) \;=\; \beta(h_2(t)^{\eta}h_1(t)-h_1(t)^{\eta}h_2(t)). \tag{21}$$

Differentiating $\frac{h_1(t)}{h_2(t)}$ as above and substituting (18) and rearranging, we find that the ratio $\frac{h_1(t)}{h_2(t)}$ satisfies the differential equation:

$$\left(\frac{h_1}{h_2}\right)' \;=\; \beta h_2^{\eta-1}\left(\left(\frac{h_1}{h_2}\right)-\left(\frac{h_1}{h_2}\right)^{\eta}\right). \tag{22}$$

Therefore, if $\frac{h_1(0)}{h_2(0)}=1$ we conclude that $\frac{h_1(t)}{h_2(t)}=1$ for all $t\geq 0$, i.e the amount in spot one always equals the amount in spot two. On the other hand, if $\frac{h_1(0)}{h_2(0)}<1$, then the right hand side of (19) is strictly negative at $t=0$ so the ratio will decrease. Since $\eta<1$ and h_2 must be bounded above by H_o, the coefficient $h_2^{\eta-1}$ can not become arbitrarily small. It follows that $h_1(t)\to 0$ at some finite time. Similarly, if $\frac{h_1(0)}{h_2(0)}>1$, then the right hand side of (19) is positive so the ratio will increase. By considering the differential equation for $\frac{h_2(t)}{h_1(t)}$, one sees, by the argument used above, that $h_2(t)\to 0$ at a finite time.

These calculations show that if the two spots start with equal amounts of Bem1p-GFP-Snc2p then the two spots will always have equal amounts. However, if one spot starts with a larger amount than the other spot, the smaller spot will vanish in finite time. A complete analytical proof of the behavior of all orbits of the system (9)-(12) is beyond the scope of this short supplement. Machine computations show that for all positive choices of the constants $\alpha,\beta,\gamma,\delta$, any $0<\eta<1$, and any initial condition whose components are strictly positive, the behavior is as follows:

(a) If $h_1(0)=h_2(0)>0$, the orbit approaches $(h_o,h_o,\frac{\beta}{\delta}2h_o^{\eta},\frac{\gamma}{\alpha}2h_o+\frac{\beta}{\alpha}2h_o^{\eta})$.

(b) If $h_1(0) > h_2(0) > 0$, the orbit approaches $(h_{oo}, 0, \frac{\beta}{\delta}h_{oo}^{\eta}, \frac{\gamma}{\alpha}h_{oo} + \frac{\beta}{\alpha}h_{oo}^{\eta})$.

(c) If $0 < h_1(0) < h_2(0)$, the orbit approaches $(0, h_{oo}, \frac{\beta}{\delta}h_{oo}^{\eta}, \frac{\gamma}{\alpha}h_{oo} + \frac{\beta}{\alpha}h_{oo}^{\eta})$.

Parameter Estimation. We used five experimental observations to derive rough estimates for the model parameters, assuming that single-focus polarized cells reflect the final model steady state.

First, Western blotting (Fig. 2B) suggests that Bem1p-GFP-Snc2p is about half as abundant as Bem1p, which is estimated to be present at about 6000 copies/cell (Ghaemmaghami et al., 2003). Thus, we estimate $H_o = 3000$.

Second, about 30% of the total v-SNARE pools are estimated to be internal (Galan et al., 2001). With similar estimates for Bem1p-GFP-Snc2p, we get $h_i = 900, h_1 + h_m = 2100$.

Third, examination of confocal slices suggests that Bem1p-GFP-Snc2p is about 5 times more concentrated in the focus than it is in the general cell membrane (Fig. S2). The area of a focus with radius $0.5\mu m$ is 1% of the total surface area of a yeast cell with radius $2.5\mu m$. Thus, $h_1 = 100$ and $h_m = 2000$ at steady state.

Fourth, we can estimate the rate of Bem1p-GFP-Snc2p delivery to a focus from internal pools from the 35 s half-time of fluorescence recovery in the FRAP data of Fig. 1D, as $0.5h_1 \times 35 = \alpha h_i$. Thus, we get $\alpha = 0.0016s^{-1}$.

Fifth, endocytosis is much more active in the focus than in the general membrane, as revealed by the concentration of actin patches at the focus. Based on previous estimates (Marco et al., 2007), we set $\gamma = 40\delta$.

Substituting the steady-state values into (13) and (14), and assuming $\eta = 0.5$, we get :

$\alpha = 0.0016$
$\beta = 0.048$
$\gamma = 0.0095$
$\delta = 0.00024$

Similar parameter estimates were generated for other values of η. Machine computation of the evolution of h_1, h_2, h_m, and h_i from given starting conditions was performed using MatLab. We re-emphasize that the model is only designed for the situation when the concentration of Bem1p-GFP-Snc2p in the two foci is higher than that in the general membrane: it is intended to model competition between established foci but not initial establishment of the foci.

Modeling Competition with Diffusion-Mediated Amplification

Our model for the diffusion-mediated amplification loop is adapted from that of Goryachev and Pokhilko (2008) (see Fig. 7B). That model dealt with a system explicitly containing Cdc42p (called RD when GDP-bound or RT when GTP-bound), a stable Bem1p-Cdc24p complex (called E_m at the membrane or E_c in the cytoplasm), and the cytoplasmic GDI Rdi1p (called I). The Bem1p-Cdc24p complex at the membrane had low basal GEF activity, catalyzing conversion of GDP-Cdc42p to GTP-Cdc42p. However, the complex could also bind GTP-Cdc42p at the membrane to generate a new species, called M, with 100-fold higher GEF activity. The GDI could bind GDP-Cdc42p at the membrane to form a complex called RDI_m, which could move from the membrane to the cytoplasm, becoming RDI_c. GAPs were not explicitly modeled, but their actions were subsumed within a rate constant k_{-2} for conversion of GTP-Cdc42p to GDP-Cdc42p. Applying mass action and assuming a rapid diffusion constant D_c for cytoplasmic species and a slow diffusion constant D_m for membrane-bound species, the dynamics of the system were modeled by the following equations:

$$
\begin{aligned}
\frac{\partial RT}{\partial t} &= (k_2 E_m + k_3 M)\cdot RD - k_{-2} RT - k_4 E_m \cdot RT + k_{-4} M - k_7 E_c \cdot RT + D_m \Delta RT \\
\frac{\partial M}{\partial t} &= k_4 E_m \cdot RT - k_{-4} M + k_7 E_c \cdot RT + D_m \Delta M \\
\frac{\partial E_m}{\partial t} &= k_1 E_c - k_{-1} E_m - k_4 E_m \cdot RT + k_{-4} M + D_m \Delta E_m \\
\frac{\partial E_c}{\partial t} &= \eta[k_{-1} E_m - (k_1 + k_7 RT) E_c] + D_c \Delta E_c \\
\frac{\partial RD}{\partial t} &= k_{-2} RT - (k_2 E_m + k_3 M)\cdot RD + k_{-6} RDI_m - k_6 I \cdot RD + D_m \Delta RD \\
\frac{\partial RDI_m}{\partial t} &= k_6 I \cdot RD - k_{-6} RDI_m + k_5 RDI_c - k_{-5} RDI_m + D_m \Delta RDI_m \\
\frac{\partial RDI_c}{\partial t} &= \eta[k_{-5} RDI_m - k_5 RDI_c] + D_c \Delta RDI_c \\
\frac{\partial I}{\partial t} &= \eta[k_{-6} RDI_m - k_6 I \cdot RD] + D_c \Delta I
\end{aligned}
$$

where η is a concentration conversion factor for membrane-cytoplasm exchange that accounts for the volume difference between membrane and cytoplasmic compartments. Goryachev and Pokhilko (2008) demonstrated that this arrangement embodies a Turing-type reaction-diffusion system that would, given sufficient time, develop a single focus of GTP-Cdc42p at a random site on the membrane.

Simulating competition between foci. Machine computation was performed using C. We simulated a spherical yeast cell with diameter $6\mu m$, membrane diffusion $D_m =$

$0.0025\mu m^2 s^{-1}$ and a well-mixed cytoplasm (as discussed by Goryachev and Pokhilko (2008), this assumption does not alter model behavior because cytoplasmic diffusion is very rapid).

To simulate competition between foci containing different ratios of polarized proteins, we rescaled concentration profiles obtained from two types of simulations: a two-foci simulation (foci located at opposite ends of the cell) and a one focus simulation. By applying appropriate scaling factors to these concentration profiles we transformed the two-foci profile with protein ratio 50:50 into two-foci profiles with various protein ratios. To conserve the total cellular quantity of all proteins, we also adjusted the cytoplasmic concentrations accordingly. The scaled foci and adjusted cytoplasmic concentrations were then used as initial conditions for simulating competition. The system was solved numerically and the integrated amount of membrane-bound Bem1p ($= E_m + M$) was recorded every 20 s. Competition simulations using the original Goryachev and Pokhilko parameters are shown in Fig. S3A.

Adapting the model to account for the Bem1p-GEF-PAK complex. We believe that the relevant polarity-generating complex includes a PAK as well as Bem1p and Cdc24p, and that the PAK is the critical component that tethers the complex to pre-existing GTP-Cdc42p at the membrane (Kozubowski et al. 2008). The PAK binds to the second SH3 domain of Bem1p (Winters and Pryciak 2005), and the weak co-immunoprecipitaion of Cla4p with Bem1p (Gulli et al. 2000, Bose et al. 2001) suggests that this complex is quite unstable, consistent with other findings indicating that even the strongest SH3 domain interactions are extremely dynamic (Lee et al. 1995). The key model parameter that specifies how long the GEF activity of Cdc24p stays tethered to GTP-Cdc42p at the membrane is k_{-4}, which was set to $0.3s^{-1}$ for the stable complex modeled by Goryachev and Pokhilko (2008). Given recent quantitative analyses of SH3 domain interactions (Demers et al. 2009), we increased this dissociation rate constant 33-fold to $10s^{-1}$ to reflect dissociation of the PAK-Bem1p weakest link in the complex. Competition simulations using the adjusted k_{-4} display markedly faster competition (Fig. S3B), suggesting that slow dissociation of the complex was rate-limiting for competition in the original model.

Estimation of GEF and GAP activities. The original estimates of basal GEF and GAP activity were derived from biochemical analyses of recombinant proteins, which exhibit rather poor activity in vitro. It was necessary to assume that GEF activity was 100-fold more active when complexed to GTP-Cdc42p simply to get enough GTP-loading for a polarization focus to develop (Goryachev and Pokhilko, 2008). Because recombinant proteins are frequently improperly folded, and may lack modifications or binding partners that significantly enhance activity in vivo, we measured GEF and GAP activities in crude yeast lysates (25 mg/mL protein) from asynchronous yeast cultures (Fig. S4A-C). Assuming that cytosol is at 100 mg/mL protein, we extrapolate the cytosolic GDP/GTP exchange rate to be $0.0048s^{-1}$ and the cytosolic GTP hydrolysis

rate to be $0.016s^{-1}$.

Although currently lacking direct biochemical support, it has been suggested that cell-cycle regulated GAP inhibition triggers polarization (Knaus et al. 2007; Sopko et al. 2007), and that GEF stimulation (perhaps resulting from the PAK-mediated Cdc24p phosphorylation that follows when the Bem1p-GEF-PAK complex binds GTP-Cdc42p) accompanies polarization (Goryachev and Pokhilko 2006; Kozubowski et al. 2008). To assess whether GEF and GAP activities change upon polarization, we compared the activities in lysates of cells arrested in early G1 by G1 cyclin deprivation (a largely unpolarized population: Lew & Reed 1993) with those of cells induced to overexpress the G1 cyclin Cln2p (a largely hyperpolarized population: Lew & Reed 1993). We found that GAP activity was indistinguishable in the two lysates, whereas GEF activity was stimulated approximately 2-fold in the hyperpolarized versus the unpolarized cells (Fig. S4E-H).

The observed GEF stimulation could represent a 2-fold increase in activity of the entire GEF pool, or a larger increase in activity of a GEF subpopulation. The mathematical model does not differentiate GEF pools and makes the simplifying assumption that all of the GEF is in the Bem1p-GEF-PAK complex. Before polarization, the model predicts that little of the complex is bound to GTP-Cdc42p: it has basal GEF activity k_2. After polarization, the model predicts that almost all of the complex is bound to GTP-Cdc42p in the polarized cluster: it has stimulated GEF activity k_3. Given that framework, and using Goryachev and Pokhilkos estimate for the abundance of the complex ($0.017\mu M$), our data yield $k_2 = 0.16\mu M^{-1}s^{-1}$ and $k_3 = 0.35\mu M^{-1}s^{-1}$. The GAP data yield $k_{-2} = 0.016s^{-1}$.

The GAP activity estimate from the lysate experiment is almost identical to that used by Goryachev and Pokhilko. However, the GEF activity estimate is 1600-fold (basal) or 35-fold (stimulated) higher. Thus, whereas the original model developed a GTP-Cdc42p cluster containing under 3% of the total cellular Cdc42p, running the model with our estimated parameters yields a much larger GTP-Cdc42p cluster containing over 25% of the total cellular Cdc42p. This seems biologically unreasonable, because localization studies suggest that less than 5% of the total Cdc42p is in the cluster (Richman et al., 2002), and biochemical studies indicate that the amount of GTP-Cdc42p in unperturbed cells is below the detection limit and can be elevated at least 10-fold by a variety of mutations (Shimada et al. 2004; Knaus et al. 2007; Sopko et al. 2007). We conclude that our lysate experiments must either overestimate the true GEF activity (perhaps by unleashing inhibited pools during lysis) or underestimate the true GAP activity (perhaps due to incomplete extraction or inactivation during lysis). Thus, we suggest that the biochemical assay provides an upper limit for the likely GEF activity and a lower limit for the likely GAP activity.

To assess how varying the GEF/GAP rates between the limits described above would affect competition between foci, we developed two new parameter sets. In the first (high GEF/GAP), we accepted the biochemical GEF estimates ($k_2 = 0.16\mu M^{-1}s^{-1}$

and $k_3 = 0.35\mu M^{-1}s^{-1}$) and adjusted the GAP rate ($k_{-2} = 0.315s^{-1}$) so as to yield a final GTP-Cdc42p cluster containing 5% of the total Cdc42p. In the second (low GEF/GAP), we accepted the biochemical GAP estimate ($k_{-2} = 0.016s^{-1}$) and adjusted the GEF rates ($k_2 = 0.0067\mu M^{-1}s^{-1}$ and $k_3 = 0.016\mu M^{-1}s^{-1}$) so as to yield a final GTP-Cdc42p cluster containing 5% of the total Cdc42p. (Note that both parameter sets retain the increased $k_{-4} = 10s^{-1}$, preserve the observed modest GEF stimulation upon polarization, and have constant GAP activity.) Remarkably, both parameter sets yielded almost identical predictions for the competition timecourse (Fig. S3C,D), indicating that the GTP cycling flux is not rate-limiting for competition in the model. We chose to present simulation data using the high GEF/GAP parameters in Fig. 7, as we consider it more likely that lysis would lead to underestimates than overestimates of protein activities.

Factors affecting competition timescale in the diffusional model. The time taken for a two-foci situation to resolve to a single focus depends on the relative amount of polarity factors in each focus, with the resolution time climbing steeply as the relative amount approaches equality (Fig. 7 and S3). For a given ratio, it is clear that a variety of other aspects of the model will impact the speed of competition (Fig. S3). The rate at which polarity factors cycle into and out of the polarized focus will clearly impact the rate of dismantling the losing focus, and hence the duration of the competition. A variety of reactions, including GEF/GAP rates, GDI-Cdc42p binding/dissociation rates, and GTP-Cdc42p-PAK-Bem1p-GEF complex association/dissociation rates, impact these dynamics. Fig. S3 shows that complex dissociation was rate-limiting for competition in the original model, whereas GEF/GAP rates were not.

Another major factor affecting the speed of competition is the amount of GTP-Cdc42p in each focus: the larger the focus, the longer it would take to dismantle it during competition. This feature accounts for the accelerating nature of the competition plots (Fig. 7 and S3). It also largely explains why increasing the amount of Bem1p-GEF-PAK complex slows competition: cells with more complex generate foci with more GTP-Cdc42p, which take longer to dismantle during competition.

Supplementary Experimental Procedures

Strains and growth conditions. Yeast strains used in this study are listed in Table I. Standard media and methods were used for plasmid and yeast genetic manipulations. The $bem1::URA3$ (Chenevert et al., 1992) and $rsr1::HIS3$ (Schenkman et al., 2002) disruptions were as previously described. $bar1::URA3$ was generated by the one-step PCR-based method (Baudin et al., 1993) using pRS306 (Sikorski and Hieter, 1989) as template. $rsr1::TRP1$ was obtained from the John Pringle lab and was generated by the one-step PCR-based method (Baudin et al., 1993).

Strains expressing $BEM1-GFP$ at the $BEM1$ locus were created as previously described (Kozubowski et al., 2008). To generate strains expressing Bem1p-GFP-Snc2p (DLY8577), we targeted homologous recombination of a plasmid containing a C-terminal fragment of $BEM1$ fused to GFP and $SNC2$ (pDLB2823) at the wild-type $BEM1$ locus. pDLB2823 contains the previously described C-terminal fragment of $BEM1$ fused to a GFP, in which the stop codon of GFP was replaced by a linker containing a NotI site (Kozubowski et al., 2008). The entire $SNC2$ ORF was inserted between the NotI site at the end of GFP and a SalI site introduced before the stop codon and the $BEM1$ 3′ untranslated region. Integration was targeted to $BEM1$ by cutting at the unique PstI site, which results in the replacement of the endogenous $BEM1$ with $BEM1-GFP-SNC2$, followed by an adjacent $LEU2$ and promoterless C-terminal fragment of $BEM1$ (designated as $BEM1-GFP-SNC2:LEU2$). Plasmid pDLB2920, for expression of Bem1p-GFP-Snc2p^{V39A,M42A}, is identical to pDLB2823 except for the indicated mutations introduced by site-directed mutagenesis. Correct integration in one chromosome of a wild-type diploid was verified by PCR tests, and sporulation and dissection was used to derive the final strains.

For expression of Cdc3p-mCherry, pDLB3138 (YIplac128-$CDC3-mCherry$, (Tong et al., 2007)) was cut at the unique BglII site to replace $CDC3$ with $CDC3-mCherry$. pDLB3086 (YIplac211-$GIC2-PBD-RFP$, (Tong et al., 2007)) was cut with ApaI to integrate $GIC2-PBD-RFP$ at $URA3$. $SPA2-mCherry$, $ABP1-mCherry$, and $SPC42-mCherry$ were generated by the PCR-based C-terminal tagging method (Longtine et al., 1998) using pDLB2865 (pFA6a-mCherry-$ADH1_t$-kanMX6) as template. Strains expressing Bem1p-GFP from the $URA3$ locus in addition to Bem1p-GFP-Snc2p were created by integrating pACB514 cut with StuI (Butty et al., 2002).

To create strains in which GAL-dependent transcription of $SIC1^{\Delta 4p}$ was controlled by addition of β-estradiol, the synthetic transcription factor construct $GAL4DBD-hER-VP16$ was targeted for integration at $URA3$ by digestion of pPP1559 with NdeI (Takahashi and Pryciak, 2008). pDLB2738, a plasmid containing PGAL-$SIC1^{\Delta 4p}$ (in which Sic1p residues T2, T5, T33, and S76 were mutated to alanine (Verma et al., 1997)) in pRS306 (Sikorski and Hieter, 1989) was digested at the unique StuI site to target integration at the $URA3$ locus.

To overexpress Bem1p-GFP, strains were transformed with a high-copy plasmid containing $BEM1-GFP$, DLB3191. DLB3191 was constructed by subcloning the SacI-XhoI fragment containing the coding sequence of $BEM1$ fused to GFP as well as $BEM1$ promoter sequence and $3'$ untranslated region from DLB2980 (Kozubowski et al., 2008) into pRS426 (Christianson et al., 1992).

Immunoblotting. Lysis of yeast, SDS-PAGE, and immunoblotting were performed as described previously (Keaton et al., 2008). The mouse monoclonal anti-GFP antibody (Roche Diagnostics, Indianapolis, IN) was used at a 1:1,000 dilution. The anti-Cdc11 polyclonal antibody (Santa Cruz Biotechnology, Santa Cruz, CA) was used at a 1:10,000 dilution.

Analysis of growth rate and cell cycle distribution. For measurement of the population doubling time, cultures were diluted to $2x10^6$ cells/mL in YEPD and grown at 30^oC. 1 mL aliquots were fixed with 3.7% formaldehyde at 30 min intervals and sonicated. The absorbance was measured at 600 nm with a Beckman DU 640B Spectrophotometer (Beckman Coulter, Fullerton, CA).

FACS analysis was performed as previously described (Haase and Reed, 2002). Cells were fixed overnight in 70% ethanol, washed with H2O, and incubated in 2 mg/ml RNaseA (Sigma-Aldrich, St. Louis, MO) in 50 mM Tris-HCl (pH 8.0) overnight at 37^oC. Following treatment with 5 mg/ml pepsin (Sigma-Aldrich, St. Louis, MO) in 0.45% HCl (vol/vol) for 15 min, DNA was stained with Sytox Green (Invitrogen, Carlsbad, CA) in 50 mM Tris-HCl (pH 7.5). DNA content of 10,000 cells was measured with a Becton Dickinson FACScan and analyzed with CellQuest software (Becton Dickinson Biosciences, San Jose, CA).

Bud scar and birth scar staining. To visualize bud and births scars, cells were fixed in 3.7% formaldehyde for 1 h at room temperature, washed, and resuspended in immunofluorescence solution B (0.1 M KPO4, pH 7.5, and 1.2 M sorbitol). Birth scars were stained with $12.5\mu g/ml$ Alexa 594ConA (Invitrogen, Carlsbad, CA) in immunofluorescence solution B for 20 min at room temperature. Bud scars were stained with a solution of 0.05% Calcofluor (Sigma-Aldrich, St. Louis, MO) for 30 min at room temperature. Cells were examined using an AxioImager.A1 (Carl Zeiss, Inc., Thornwood, NY) with a 100x/1.4 Plan Apochromat oil immersion objective. Images were captured using an ORCA cooled charge-coupled device camera (Hamamatsu, Bridgewater, NJ) and interfaced with MetaMorph software (Universal Imaging, Silver Spring, MD). Images were processed for presentation using Photoshop (Adobe systems, San Jose, CA).

Actin staining. Cells were grown overnight in synthetic complete medium with dextrose at 24^oC. EM grade formaldehyde (Polysciences, Warrington, PA) was added to the culture to a final concentration of 4% for 10 min at room temperature with shaking. The cells were pelleted, resuspended in PBS with 4% formaldehyde and incubated with

shaking for 1 h at 24^{o}C. The cells were then washed twice with PBS. 180μL of fixed cells were incubated with 20μL Rhodamine phalloidin (Invitrogen) for 1 h with vortexing every 15 min, then washed 5 times with PBS and resuspended in 100μL mounting medium. Cells were examined using an AxioObserver.Z1 (Zeiss) with a 100x/1.4 Plan Apochromat oil immersion objective. Images were captured using a Coolsnap ES2 high resolution CCD camera (Photometrics).

Centrifugal elutriation. Enrichment of small daughter cells from exponentially growing cultures was achieved by centrifugal elutriation as described previously (Lew and Reed, 1993). After elutriation, cells were grown in rich medium YEPD at 37^{o}C for 80 min or 180 min. Samples were fixed with 3.7% formaldehyde for 1 h at room temperature, washed once and resuspended in immunofluorescence solution B. Birth scars were stained as described above.

Live cell microscopy. For live-cell imaging exponentially growing cells were mounted on a slide with a slab of synthetic medium solidified with 2% agarose (Denville Scientific, Inc., Metuchen, NJ). Images in Figures 1E and 2C were acquired using the AxioImager system described above. Images in Figures 4-7 were acquired using an Axio Observer.Z1 (Zeiss) with a 100x/1.4 Plan Apochromat oil immersion objective controlled by MetaMorph software (Universal Imaging). Images were captured using a QuantEM backthinned EM-CCD camera (Photometrics). All timelapses consisted of DIC and fluorescence (GFP and, where indicated, RFP) images acquired over 11 z-planes with 0.5μm steps.

Deconvolution and Image Analysis. Image deconvolution was performed using Huygens Essential software (Scientific Volume Imaging, Hilversum, The Netherlands). Image analysis was performed using Metamorph (Universal Imaging) and Volocity (Improvision, Inc., Waltham, MA) software.

For timelapse series, fluorescence images were deconvolved with the Huygens SVI batch processor using the classic maximum likelihood estimation and predicted point-spread function using a constant background across all images from the same day, with a signal to noise ratio of 5 and a maximum of 40 iterations. The output format was 16-bit, unscaled images to enable comparison of pixel values across images. Maximum intensity projections were constructed to facilitate observation of polarization foci in different focal planes. The resultant deconvolved timelapses were then scored visually for the formation of multiple GFP or mCherry foci, for the duration of focus competition, and for the time of onset of polarization. For comparison of the interval between GFP polarization and budding, as well as the duration of competition between foci, a focus was scored as being present as soon (or as long) as it was detectable above background by visual inspection.

For Fig.s 1E and 2C, representative individual cells were cropped out of larger fields and compiled into a single image using Photoshop (Adobe Systems). Single z-plane

images were deconvolved using the classic maximum likelihood estimation and predicted point-spread function using a constant background setting across all images of the same fluorophore (either GFP or td Tomato), with a signal to noise ratio of 10 and a maximum of 40 iterations.

Quantitation of GTP-Cdc42p polarization in wild-type and re-wired cells. To minimize imaging variability, re-wired ($BEM1-GFP-SNC2, PBD-RFP, rsr1\Delta$) and wild-type ($BEM1-GFP, PBD-RFP, rsr1\Delta$) cells were mixed and imaged on the same slide. To distinguish the two genotypes, cells were grown separately at 30^oC in synthetic complete medium and 10^7 cells of each genotype were pelleted and resuspended in either water (DLY 9826) or water containing 1 mg/mL Alexa 488-Concanavalin-A (Invitrogen) (DLY9831) for 2 min. The cells were then washed twice in synthetic medium, mixed together, and mounted on the same slab of synthetic medium solidified with agarose. Fields of cells containing both genotypes (as determined by the Alexa 488 signal) were imaged using the AxioObserver system described above. RFP images were acquired for 21 z-planes with $0.5\mu m$ steps, and pixel values (divided by 10 using Metamorph) were deconvolved in the Huygens SVI batch processor using the classic maximum likelihood estimation and predicted point-spread function using a constant background across all images, with a signal to noise ratio of 15 and a maximum of 40 iterations. PBD-RFP probe polarization was quantified using Volocity by setting a threshold to select either the entire cell or only the polarized signal, after which the summed intensity of the PBD-RFP signal was recorded for unbudded and small-budded cells. To account for cell-to-cell variations in PBD-RFP abundance, the proportion of the total cellular PBD-RFP signal that was polarized was calculated for each cell.

Quantitation of GFP and actin patch polarization in wild-type and re-wired cells. To quantitate polarization of Bem1p-GFP or Bem1p-GFP-Snc2p, the position and integrated intensity of the GFP signal was measured from deconvolved images using Volocity with a threshold set to select only the polarized signal. The summed intensity, as well as the centroid in X, Y, and Z of the polarized signal, was recorded for each timepoint. For competing foci, we recorded the summed intensity during the interval from initial detection of two foci until only a single focus remained detectable by the threshold.

To quantify actin patch polarization, cells containing Abp1p-mCherry were imaged and deconvolved as described above, and a threshold was identified using Volocity that would select the actin patches. The centroid and summed intensity of each actin patch (or group of patches, when they were very close together) was recorded. For each timepoint, the intensity of every actin patch/patch cluster (i.e. object identified by thresholding) whose centroid was within $2\mu m$ of the centroid of the polarized GFP signal was summed to compute a total polarized actin patch intensity. The polarized actin patch intensity and polarized GFP intensity were plotted as a percentage of the peak intensity prior to budding (budding was determined from the DIC images). To

measure the interval between polarization of GFP and polarization of actin patches, the GFP or actin patch signal was determined to be polarized when the summed intensity reached 50% of peak. The same time was used to determine the interval between actin patch polarization and bud emergence (scored from DIC images).

Photobleaching. Cells were mounted on 2% agarose slides and imaged on a SP5 confocal microscope (Leica Microsystems, Bannockburn, IL) using a 63x/1.20 water Plan Apochromat objective. Photobleaching experiments were done using the FRAPwizard in the Leica LAS AF software with 1 iteration of bleaching at 100% laser power and image acquisition at 4% power using an Argon/2 (488) laser. The data shown in Figure 1C were first normalized to pre-bleach signal intensity and then averaged over several experiments. The recovery half-times were calculated from individual curve fits to the normalized data using Kaleidagraph (Synergy Software, Reading, PA). FRAP analysis was performed on small-budded cells with a strong polarized signal, and the bleached zone encompassed the distal 50% of the bud. The partial recovery for Bem1p-GFP-Snc2p likely reflects bleaching of a significant fraction of the total fluorescent protein, as recycling compartments are enriched in the bud.

Latrunculin Treatment. Exponentially growing cells were treated with $200\mu M$ Latrunculin A (Invitrogen) in complete synthetic medium with dextrose at 30^oC for 2 h. As reported previously, this concentration suffices to depolymerize all detectable F-actin (both cables and patches) within 5 min (Ayscough et al., 1997). The cells were then mounted for live-cell microscopy on slabs containing $200\mu M$ Latrunculin A. Cells were imaged using the AxioObserver.Z1 system described above at 30^oC. Single images were acquired and representative cells were assembled into a montage. For quantification of cells containing PBD-RFP and either Bem1p-GFP-Snc2p or Bem1p-GFP, 11 z-planes with $0.5\mu m$ steps were acquired through the cells and the presence or absence of a polarized signal was scored from these images.

Sic1p induction. Overexpression of Sic1p lacking 4 phosphorylation sites was induced by addition of 75 nM β-estradiol (Sigma-Aldrich). For live cell filming, Sic1p was induced for 30 min in exponentially growing cells in synthetic complete medium with 2% dextrose at 30^oC. Cells were then mounted for live-cell microscopy on slabs containing 75 nM β-estradiol and imaged at 30^oC using the Axio Observer system described above. GFP and DIC images were acquired for 11 z-planes with $0.5\mu m$ steps every 2 min. Maximum intensity projections of the GFP planes were created for each timepoint.

Assay for GEF and GAP activities in total cell lysates. Yeast lysates were prepared in lysis buffer (25 mM Tris-HCl pH 7.5, 1 mM EDTA, 5 mM $MgCl_2$, 150 mM NaCl, 0.5% NP-40, 2 mM DTT, 1 mM $Na_4P_2O_7$, 5 mM Na_3VO_4, 2 mM PMSF, and $20\mu g/mL$ each of pepstatin, leupeptin, aprotinin, and benzamidine) by passing the cells three times through a French Press at 1000 psi. Lysates were clarified by centrifugation

at 14000 rpm for 5 min at 4^oC in an Eppendorf microcentrifuge. Recombinant yeast GST-Cdc42p was purified from baculovirus-infected Sf9 cells using glutathione beads as described for human Cdc42p (Cerione et al., 1995). For GEF assays, GST-Cdc42p was pre-incubated for 30 min at 20^oC with 3000 cpm/pmol $\alpha-^{32}$P-GDP in loading buffer (25 mM Tris-HCl pH 7.5, 1 mM EDTA, 5 mM $MgCl_2$, 2 mM DTT, 200 mM $(NH_4)_2SO_4$, $5\mu M$ GDP, 2 mM PMSF, and $10\mu g/mL$ each of pepstatin, leupeptin, aprotinin, and benzamidine). For GAP assays, GST-Cdc42p was pre-loaded with $\gamma-^{32}$P-GTP in the same buffer (with $5\mu M$ GTP instead of GDP). Beads containing appropriately loaded GST-Cdc42p were washed three times with 1 mL of wash buffer (25 mM Tris-HCl pH 7.5, 10 mM $MgCl_2$, 2 mM DTT, $5\mu M$ GDP, and $10\mu g/mL$ each of pepstatin, leupeptin, aprotinin, and benzamidine), and incubated with lysate ($10\mu L$ of a 10% bead slurry and $40\mu L$ lysate = 1 mg total protein used per timepoint) for the indicated time at 25^oC. Samples were rapidly chilled, filtered onto $0.45\mu m$ filters, and washed to detect protein-bound radioactivity as described (Hart et al., 1991). Western blotting confirmed that the GST-Cdc42p remained intact during these experiments (not shown). We estimate that the GST-Cdc42p loading yielded 0.3-0.5 mol of bound nucleotide per mol Cdc42p, and exchange/hydrolysis rates were exponential for the first 10 min of the assay.

Cell synchronization by G1 cyclin deprivation or overproduction. For GEF and GAP assays of primarily unpolarized cells, cultures of a $cln1\Delta, cln2\Delta, cln3\Delta, GAL1-CLN3$ strain (DLY222) were grown in galactose-containing medium and arrested by addition of 2% dextrose for >4 h (at which point >95% of cells were unbudded) prior to harvesting and lysis. For assays of hyper-polarized cells, cultures of a $GAL1-CLN2$ strain (DLY232) were grown in sucrose-containing medium and induced by addition of 2% galactose for >4 h (at which point >95% of cells had elongated buds). Control experiments showed that similar medium shifts for wild-type cells did not affect GEF and GAP activities.

Supplementary Figure Legends

Fig. S1. Cell cycle arrest at a polarized stage does not allow Bem1p-GFP-Snc2p to initiate additional buds. (A) Exponentially growing cells expressing either Bem1p-GFP (open symbols) or Bem1p-GFP-Snc2p (closed symbols) were induced to overexpress Sic1p by the addition of 75 nM β-estradiol. This stabilized form of the CDK inhibitor Sic1p blocks the cells in late G1 with polarized actin, leading to the formation of elongated buds; with time, cells re-polarize to make a second (and eventually more) elongated bud (Verma et al., 1997). Aliquots (1 mL) were taken every hour and fixed with 3.7% formaldehyde. Cells were scored for number of buds by DIC microscopy. n>1000. The percentage of budded cells with 2 buds is shown, and indicates that Bem1p-GFP-Snc2p did not promote re-budding during the arrest. (B) Frames from GFP timelapse of a cell expressing Bem1p-GFP-Snc2p and Sic1p. Elapsed time is shown as h:min. Bar = 2 μm.

Fig. S2. Estimating the relative concentration of Bem1p-GFP-Snc2p in the polarized spot and the general membrane. A sample medial confocal section through a live $BEM1-GFP-SNC2$ diploid cell mounted on a 2% agarose slab and imaged using a Leica SP5 confocal microscope with a 63x/1.20 water Plan Apochromat objective. The fluorescence intensity at the polarized spot relative to the non-polarized membrane was quantitated.

Fig. S3. Effect of varying parameters on simulated competition during diffusion-mediated polarization. (A) Simulated competition using the parameter set of Goryachev and Pokhilko (2008). (B) Simulated competition with an increased dissociation rate to reflect the instability of the Bem1p-GEF-PAK complex. (C) Simulated competition with high GEF/GAP parameters. (D) Simulated competition with low GEF/GAP parameters. (E) Summary of the parameter sets employed.

Fig. S4. Measurement of Cdc42p guanine nucleotide exchange and hydrolysis in yeast cell lysates. (A) GEF Assay: Baculovirus-produced recombinant Cdc42p pre-loaded with $\alpha-^{32}$P-GDP was incubated together with buffer alone (open circles) or with crude lysate (25 mg/ml total protein) made by French Press extraction of asynchronous wild-type yeast cells followed by centrifugation to remove cell debris (filled circles). Protein-bound radioactivity was quantitated by a nitrocellulose filtration assay in triplicate samples. A representative experiment is shown, indicating that lysate GEFs accelerated release of GDP from Cdc42p. (B) GAP Assay: Cdc42p was pre-loaded with $\gamma-^{32}$P-GTP and assayed as above. (C) Average rates of GDP release from Cdc42p (as in A) and GTP hydrolysis by Cdc42p (as in B), from six independent experiments. (D) Cdc42p was pre-loaded with GTP-$\gamma-^{35}$S (a slowly-hydrolyzable GTP analogue) and assayed as in A, B. As expected, this nucleotide remained bound to Cdc42p even after 1 h of incubation with lysate (note different time-scale relative to A,B), indicating that

Cdc42p remains intact upon incubation with lysate, and that the release of radioactivity documented in A, B was not due to proteolysis or denaturation of the Cdc42p, or to GTP release, but truly reflected GDP release or GTP hydrolysis. (E-H) GEF and GAP activity in lysates from cells lacking ($cln-$) or overexpressing ($CLN+$) G1 cyclins. (E) GEF assay: GDP release from Cdc42p upon incubation with lysates from $cln1, cln2, cln3$ cells arrested in dextrose medium (open circles) or $GAL1-CLN2$ cells grown in galactose medium (filled circles). A representative experiment is shown. Dashed line: GDP release in the absence of lysate. (F) Average rates of GDP release for six independent experiments. The difference in GEF activity is statistically significant ($P < 0.01$ using the Student's t-test). Control experiments confirmed that these differences were due to the G1 cyclin perturbation and not to differences in the media. (G) GAP assay: GTP hydrolysis by Cdc42p with the same lysates. A representative experiment is shown. (H) Average rates of GTP hydrolysis for six independent experiments.

Fig. S5. Competition in Bem1p-overexpressing cells: an underdog wins. $SPA2-mCherry$ cells carrying a high-copy $BEM1-GFP$ plasmid were filmed as in Fig. 7. In this case, what appeared to be a clearly stronger focus at one timepoint (arrow) then disappeared while the initially weaker focus (arrowhead) grew to become the bud site. Bar = 2 μm.

Fig. S6. Apparent relocation of a focus in Bem1p-overexpressing cells. $SPA2-mCherry$ cells carrying a high-copy $BEM1-GFP$ plasmid were filmed as in Fig. 7. In this case, a clear single focus (arrow) disappeared while another (arrowhead) appeared and grew to become the bud site. This may be analogous to the situation in Fig. S5, but with the weaker focus being undetectable at the earlier timepoint. Bar = 2 μm.

Fig. S7. Apparent merging of nearby foci in Bem1p-overexpressing cells. $SPA2-mCherry$ cells carrying a high-copy $BEM1-GFP$ plasmid were filmed as in Fig. 7. In this case, two weak foci in close proximity arise (arrows), and a single focus located in between goes on to become the bud site. Bar = 2 μm.

Supplementary Movie Legends

Movie 1. Polarization of Bem1p-GFP-Snc2p and Abp1p-mCherry. $BEM1-GFP-SNC2, ABP1-mCherry, rsr1\Delta$ homozygous diploid cells were imaged at 24^{o}C using a Zeiss AxioObserver microscope. GFP, RFP and DIC images were acquired at 11 z-planes with $0.5\mu m$ steps every 1.5 min. Maximum intensity projections of the deconvolved fluorescence images and selected DIC images are shown. Bar = $2\mu m$.

Movie 2. Polarization of Bem1p-GFP and Abp1p-mCherry. $BEM1-GFP, ABP1-mCherry, rsr1\Delta$ homozygous diploid cells were imaged at 24^{o}C using a Zeiss AxioObserver microscope. GFP, RFP and DIC images were acquired at 11 z-planes with $0.5\mu m$ steps every 1.5 min. Maximum intensity projections of the deconvolved fluorescence images and selected DIC images are shown. Bar = $2\mu m$.

Movie 3. Re-wired cells can grow 2 buds simultaneously. A $BEM1-GFP-SNC2, rsr1\Delta$ homozygous diploid mother-daughter pair was imaged at 24^{o}C using a Zeiss Axio Observer microscope. GFP and DIC images were acquired at 11 z-planes with $0.5\mu m$ steps every 1.5 min. Maximum intensity projections of the deconvolved fluorescence images and selected DIC images are shown. Bar = $2\mu m$.

Movie 4. Re-wired cells can grow 2 buds simultaneously. $BEM1-GFP-SNC2, RSR1$ haploid cells were imaged at 24^{o}C using a Zeiss Axio Imager microscope. DIC images were acquired at 11 z-planes with $0.5\mu m$ steps every 30 s. The best focal plane at each timepoint was selected and assembled into a timelapse. The middle cell also has a single bud, but it is growing out of the selected focal plane and not visible in these images. Bar = $2\mu m$.

Movies 5 and 6. Competition between foci in re-wired cells. $BEM1-GFP-SNC2, rsr1\Delta$ homozygous diploid cells were imaged at 30^{o}C using a Zeiss AxioObserver microscope. GFP and DIC images were acquired at 11 z-planes with $0.5\mu m$ steps every 1.5 min. Maximum intensity projections of the deconvolved GFP images are shown. Bar = $2\mu m$.

Movie 7. Competition between foci in cells overexpressing Bem1p. $SPA2-mCherry$ cells carrying a high-copy $BEM1-GFP$ plasmid were imaged at 30^{o}C using a Zeiss AxioObserver microscope. mCherry and DIC images were acquired at 11 z-planes with $0.5\mu m$ steps every 1.5 min. Maximum intensity projections of the GFP images are shown. Bar = $2\mu m$.

Movie 8. Cells overexpressing Bem1p can grow 2 buds simultaneously. Cells carrying a high-copy $BEM1-GFP$ plasmid were imaged at 30^{o}C using a Zeiss AxioObserver microscope. GFP and DIC images were acquired at 11 z-planes with $0.5\mu m$

steps every 1.5 min. Maximum intensity projections of the GFP images are shown. Bar $= 2\mu m$.

References

Ayscough, K.R., J. Stryker, N. Pokala, M. Sanders, P. Crews, and D.G. Drubin. 1997. High rates of actin filament turnover in budding yeast and roles for actin in establishment and maintenance of cell polarity revealed using the actin inhibitor latrunculin-A. *J. Cell Biol.* 137:399-416.

Baudin, A., O. Ozier-Kalogeropoulos, A. Denouel, F. Lacroute, and C. Cullin. 1993. A simple and efficient method for direct gene deletion in *Saccharomyces cerevisiae*. *Nucleic Acids Res.* 21:3329-3330.

Bose, I., J.E. Irazoqui, J.J. Moskow, E.S. Bardes, T.R. Zyla, and D.J. Lew. 2001. Assembly of scaffold-mediated complexes containing Cdc42p, the exchange factor Cdc24p, and the effector Cla4p required for cell cycle-regulated phosphorylation of Cdc24p. *J Biol Chem*. 276:7176-86.

Butty, A.C., N. Perrinjaquet, A. Petit, M. Jaquenoud, J.E. Segall, K. Hofmann, C. Zwahlen, and M. Peter. 2002. A positive feedback loop stabilizes the guanine-nucleotide exchange factor Cdc24 at sites of polarization. *Embo J*. 21:1565-1576.

Cerione, R.A., D. Leonard, and Y. Zheng. 1995. Purification of baculovirus-expressed Cdc42Hs. *Methods Enzymol*. 256:11-5.

Chenevert, J., K. Corrado, A. Bender, J. Pringle, and I. Herskowitz. 1992. A yeast gene (*BEM1*) necessary for cell polarization whose product contains two SH3 domains. *Nature*. 356:77-79.

Christianson, T.W., R.S. Sikorski, M. Dante, J.H. Shero, and P. Hieter. 1992. Multifunctional yeast high-copy-number shuttle vectors. *Gene*. 110:119-22.

Demers, J.P., and A. Mittermaier. 2009. Binding mechanism of an SH3 domain studied by NMR and ITC. *J Am Chem Soc*. 131:4355-67.

Galan, J.M., A. Wiederkehr, J.H. Seol, R. Haguenauer-Tsapis, R.J. Deshaies, H. Riezman, and M. Peter. 2001. Skp1p and the F-box protein Rcy1p form a non-SCF complex involved in recycling of the SNARE Snc1p in yeast. *Mol Cell Biol*. 21:3105-17.

Ghaemmaghami, S., W.K. Huh, K. Bower, R.W. Howson, A. Belle, N. Dephoure, E.K. O'Shea, and J.S. Weissman. 2003. Global analysis of protein expression in yeast. *Nature*. 425:737-41.

Goryachev, A.B., and A.V. Pokhilko. 2006. Computational model explains high activity and rapid cycling of Rho GTPases within protein complexes. *PLoS Comput Biol*. 2:e172.

Goryachev, A.B., and A.V. Pokhilko. 2008. Dynamics of Cdc42 network embodies a Turing-type mechanism of yeast cell polarity. *FEBS Lett*. 582:1437-1443.

Grote, E., G. Vlacich, M. Pypaert, and P.J. Novick. 2000. A snc1 endocytosis mutant: phenotypic analysis and suppression by overproduction of dihydrosphingosine phosphate lyase. *Mol Biol Cell*. 11:4051-65.

Gulli, M.P., M. Jaquenoud, Y. Shimada, G. Niederhauser, P. Wiget, and M. Peter. 2000. Phosphorylation of the Cdc42 exchange factor Cdc24 by the PAK-like kinase Cla4 may regulate polarized growth in yeast. *Mol. Cell*. 6:1155-1167.

Haase, S.B., and S.I. Reed. 2002. Improved flow cytometric analysis of the budding yeast cell cycle. *Cell Cycle*. 1:132-6.

Hart, M.J., K. Shinjo, A. Hall, T. Evans, and R.A. Cerione. 1991. Identification of the human platelet GTPase activating protein for the CDC42Hs protein. *J Biol Chem*. 266:20840-8.

Keaton, M.A., L. Szkotnicki, A.R. Marquitz, J. Harrison, T.R. Zyla, and D.J. Lew. 2008. Nucleocytoplasmic trafficking of G2/M regulators in yeast. *Mol Biol Cell*. 19:4006-18.

Knaus, M., M.P. Pelli-Gulli, F. van Drogen, S. Springer, M. Jaquenoud, and M. Peter. 2007. Phosphorylation of Bem2p and Bem3p may contribute to local activation of Cdc42p at bud emergence. *EMBO J*. 26:4501-13.

Kozubowski, L., K. Saito, J.M. Johnson, A.S. Howell, T.R. Zyla, and D.J. Lew. 2008. Symmetry-Breaking Polarization Driven by a Cdc42p GEF-PAK Complex. *Curr Biol*. 18:1719-26.

Lee, C.H., B. Leung, M.A. Lemmon, J. Zheng, D. Cowburn, J. Kuriyan, and K. Saksela. 1995. A single amino acid in the SH3 domain of Hck determines its high affinity and specificity in binding to HIV-1 Nef protein. *Embo J*. 14:5006-15.

Lew, D.J., and S.I. Reed. 1993. Morphogenesis in the yeast cell cycle: regulation by Cdc28 and cyclins. *J. Cell Biol.* 120:1305-1320.

Longtine, M.S., A. McKenzie III, D.J. DeMarini, N.G. Shah, A. Wach, A. Brachat, P. Philippsen, and J.R. Pringle. 1998. Additional modules for versatile and economical PCR-based gene deletion and modification in *Saccharomyces cerevisiae*. *Yeast*. 14:953-961.

Marco, E., R. Wedlich-Soldner, R. Li, S.J. Altschuler, and L.F. Wu. 2007. Endocytosis optimizes the dynamic localization of membrane proteins that regulate cortical polarity. *Cell*. 129:411-22.

Protopopov, V., B. Govindan, P. Novick, and J.E. Gerst. 1993. Homologs of the synaptobrevin/VAMP family of synaptic vesicle proteins function on the late secretory pathway in S. cerevisiae. *Cell*. 74:855-61.

Pruyne, D.W., D.H. Schott, and A. Bretscher. 1998. Tropomyosin-containing actin cables direct the Myo2p-dependent polarized delivery of secretory vesicles in budding yeast [In Process Citation]. *J Cell Biol*. 143:1931-45.

Richardson, H.E., C. Wittenberg, F. Cross, and S.I. Reed. 1989. An essential G1 function for cyclin-like proteins in yeast. *Cell*. 59:1127-1133.

Richman, T.J., M.M. Sawyer, and D.I. Johnson. 2002. Saccharomyces cerevisiae Cdc42p localizes to cellular membranes and clusters at sites of polarized growth. *Eukaryot Cell*. 1:458-68.

Schenkman, L.R., C. Caruso, N. Page, and J.R. Pringle. 2002. The role of cell cycle-regulated expression in the localization of spatial landmark proteins in yeast. *J Cell Biol*. 156:829-41.

Shimada, Y., P. Wiget, M.P. Gulli, E. Bi, and M. Peter. 2004. The nucleotide exchange factor Cdc24p may be regulated by auto-inhibition. *Embo J*. 23:1051-62.

Sikorski, R.S., and P. Hieter. 1989. A system of shuttle vectors and yeast host strains designed for efficient manipulation of DNA in *Saccharomyces cerevisiae*. *Genetics*. 122:19-27.

Sopko, R., D. Huang, J.C. Smith, D. Figeys, and B.J. Andrews. 2007. Activation of the Cdc42p GTPase by cyclin-dependent protein kinases in budding yeast. *EMBO J*. 26:4487-500.

Takahashi, S., and P.M. Pryciak. 2008. Membrane localization of scaffold proteins promotes graded signaling in the yeast MAP kinase cascade. *Curr Biol*. 18:1184-91.

Tong, Z., X.D. Gao, A.S. Howell, I. Bose, D.J. Lew, and E. Bi. 2007. Adjacent positioning of cellular structures enabled by a Cdc42 GTPase-activating protein-mediated zone of inhibition. *J Cell Biol*. 179:1375-84.

Verma, R., R.S. Annan, M.J. Huddleston, S.A. Carr, G. Reynard, and R.J. Deshaies. 1997. Phosphorylation of Sic1p by G1 Cdk required for its degradation and entry into S phase. *Science*. 278:455-60.

Wedlich-Soldner, R., S. Altschuler, L. Wu, and R. Li. 2003. Spontaneous cell polarization through actomyosin-based delivery of the Cdc42 GTPase. *Science*. 299:1231-5.

Winters, M.J., and P.M. Pryciak. 2005. Interaction with the SH3 domain protein Bem1 regulates signaling by the Saccharomyces cerevisiae p21-activated kinase Ste20. *Mol Cell Biol*. 25:2177-90.

Table I. Yeast strains

Strain	*Relevant genotype*	*Source*
DLY222[1]	**a** *cln1 cln2 cln3* P_{GAL1}*-CLN3:TRP1*	(Lew and Reed, 1993)
DLY232[1]	**a** P_{GAL1}*-CLN2:LEU2*	(Lew and Reed, 1993)
DLY5029	**a**/α *rsr1::HIS3/ rsr1::HIS3 bem1::URA3/BEM1*	(Kozubowski et al., 2008)
DLY8577	**a**/α *BEM1-GFP-SNC2:LEU2/BEM1*	This study
DLY8601	**a** *BEM1-GFP-SNC2:LEU2*	This study
DLY8666	**a** *BEM1-GFP-SNC2:LEU2 rsr1::TRP1*	This study
DLY8990	**a** *BEM1-GFP:LEU2 rsr1::TRP1*	This study
DLY9032	**a**/α *BEM1-GFP:LEU2/BEM1*	This study
DLY9069	**a** *BEM1-GFP:LEU2*	This study
DLY9122	**a**/α *BEM1-GFP-SNC2:LEU2/ BEM1-GFP-SNC2:LEU2*	This study
DLY9123	**a**/α *BEM1-GFP-SNC2:LEU2/BEM1 rsr1::TRP1/ rsr1::TRP1*	This study
DLY9124	**a**/α *BEM1-GFP-SNC2:LEU2/ BEM1-GFP-SNC2:LEU2 rsr1::TRP1/ rsr1::TRP1*	This study
DLY9198	**a**/α *BEM1-GFP:LEU2/BEM1 rsr1::TRP1/ rsr1::TRP1*	This study
DLY9200	**a**/α *BEM1-GFP:LEU2/ BEM1-GFP:LEU2 rsr1::TRP1/ rsr1::TRP1*	This study
DLY9432	α *BEM1-GFP-SNC2:LEU2 SPA2-mCherry:kan*^{R} *rsr1::TRP1*	This study
DLY9439	**a** *BEM1-GFP:LEU2 SPA2-mCherry:kan*^{R} *rsr1::TRP1*	This study
DLY9641	**a**/α *BEM1-GFP-SNC2(V39A,M42A):LEU2/BEM1 rsr1::TRP1/ rsr1::TRP1*	This study
DLY9826	α *BEM1-GFP-SNC2:LEU2 GIC2-PBD-RFP:URA3 rsr1::TRP1*	This study
DLY9831	α *BEM1-GFP:LEU2 GIC2-PBD-RFP:URA3 rsr1::TRP1*	This study
DLY10092	α *BEM1-GFP-SNC2:LEU2 CDC3-mCherry:LEU2 rsr1::TRP1*	This study
DLY10096	α *BEM1-GFP:LEU2 CDC3-mCherry:LEU2 rsr1::TRP1*	This study
DLY11123	**a**/α *BEM1-GFP-SNC2:LEU2/ BEM1-GFP-SNC2:LEU2 rsr1::TRP1/ rsr1::TRP1 SPC42-mCherry:kan*^{R}*/SPC42*	This study
DLY11227	**a**/α *BEM1-GFP-SNC2:LEU2/BEM1-GFP-SNC2:LEU2 GIC2-PBD-RFP:URA3/GIC2-PBD-RFP:URA3 rsr1::TRP1/rsr1::TRP1*	This study
DLY11229	**a**/α *BEM1-GFP-SNC2:LEU2/ BEM1-GFP-SNC2:LEU2 CDC3-mCherry:LEU2/CDC3-mCherry:LEU2 rsr1::TRP1/ rsr1::TRP1*	This study
DLY11230	**a**/α *BEM1-GFP-SNC2:LEU2/ BEM1-GFP-SNC2:LEU2*	This study

	SPA2-mCherry:kan^R/ SPA2-mCherry:kan^R rsr1::TRP1/ rsr1::TRP1 bar1::URA3/BAR1	
DLY11231	**a**/α *BEM1-GFP:LEU2/ BEM1-GFP:LEU2 rsr1::TRP1/ rsr1::TRP1* pRS426-*BEM1-GFP*	This study
DLY11242	**a**/α *BEM1-GFP-SNC2:LEU2/ BEM1-GFP-SNC2:LEU2 ABP1-mCherry:kan^R/ABP1-mCherry:kan^R rsr1::TRP1/ rsr1::TRP1*	This study
DLY11264	**a**/α *BEM1-GFP-SNC2:LEU2/ BEM1-GFP-SNC2:LEU2 rsr1::TRP1/ rsr1::TRP1 BEM1-GFP:URA3/URA3*	This study
DLY11266	**a**/α *BEM1-GFP:LEU2/ BEM1-GFP:LEU2 rsr1::TRP1/ rsr1::TRP1 BEM1-GFP:URA3/URA3*	This study
DLY11309	**a**/α *BEM1-GFP-SNC2(V39A,M42A):LEU2/BEM1 rsr1::TRP1/ rsr1::TRP1 GIC2-PBD-RFP:URA3/URA3*	This study
DLY11320	**a**/α *BEM1-GFP:LEU2/ BEM1-GFP:LEU2 ABP1-mCherry:kan^R/ABP1-mCherry:kan^R rsr1::TRP1/ rsr1::TRP1*	This study
DLY11321	**a**/α *BEM1-GFP-SNC2:LEU2/BEM1 rsr1::TRP1/ rsr1::TRP1 GIC2-PBD-RFP:URA3/URA3*	This study
DLY11322	**a**/α *BEM1-GFP-SNC2:LEU2/ BEM1-GFP-SNC2:LEU2 rsr1::TRP1/ rsr1::TRP1 P_{GAL1}-SIC1$^{\Delta 4P}$:URA3/P_{ADH1}-GAL4DBD-hER-VP16:URA3*	This study
DLY11323	**a**/α *BEM1-GFP:LEU2/ BEM1-GFP:LEU2 rsr1::TRP1/ rsr1::TRP1 P_{GAL1}-SIC1$^{\Delta 4P}$:URA3/P_{ADH1}-GAL4DBD-hER-VP16:URA3*	This study
DLY11653	**a**/α *BEM1-GFP:LEU2/ BEM1-GFP:LEU2 SPA2-mCherry:kan^R/ SPA2-mCherry:kan^R rsr1::TRP1/ rsr1::TRP1* pRS426-*BEM1-GFP*	This study

All strains are in the YEF473 background (*his3-*Δ*200 leu2-*Δ*1 lys2-801 trp1-*Δ*63 ura3-52)* except as marked below.

[1]These strains are in the BF264-15Du (Richardson et al., 1989) background (*ade1 his2 leu2-3,112 trp1-1 ura3*Δ*ns*)

[G] Supplemental Figure 1

Howell et al., Supplementary Figure 1

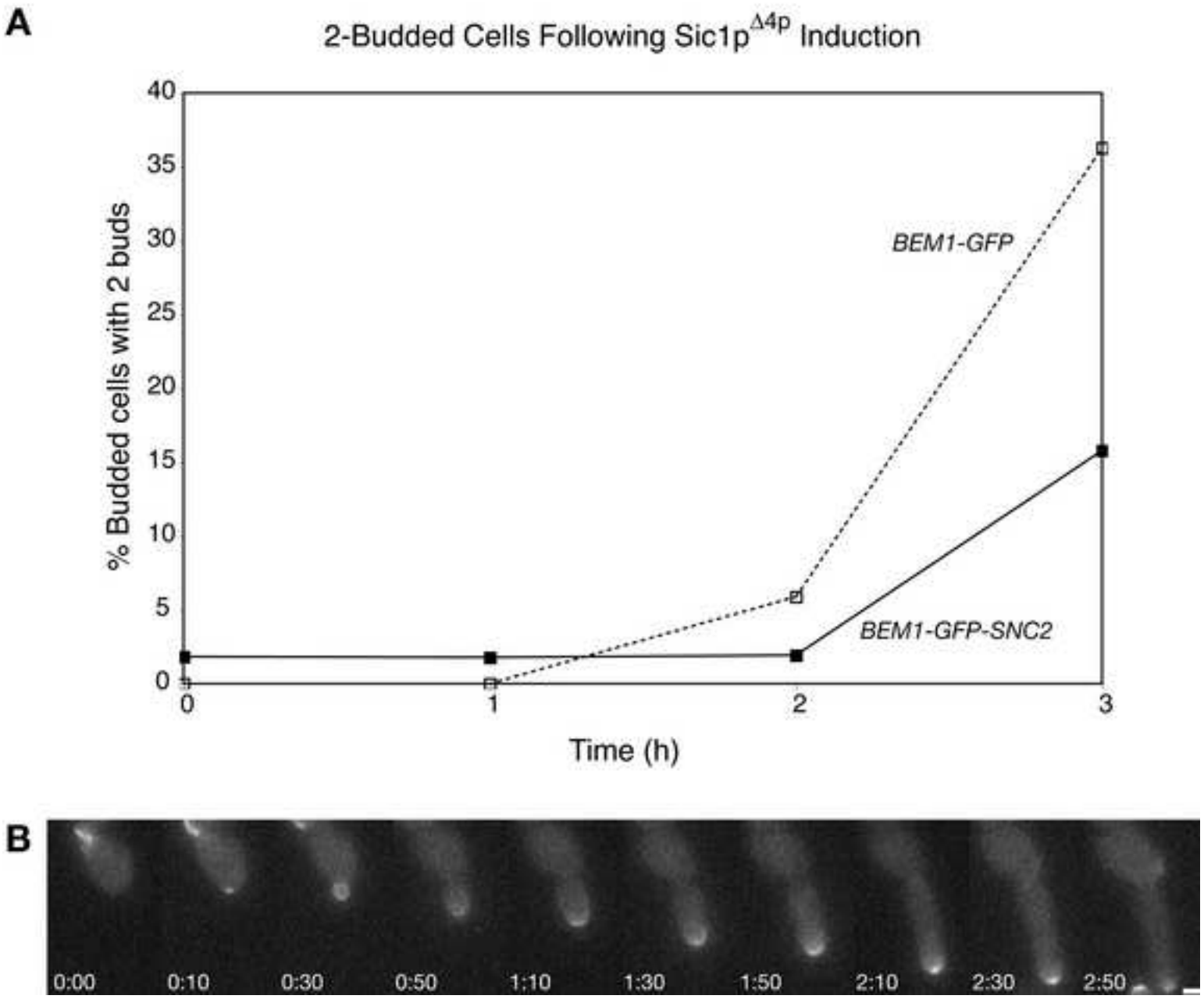

[G] Supplemental Figure 2

Howell et al., Supplementary Figure 2

BEM1-GFP-SNC2/BEM1-GFP-SNC2
RSR1/RSR1

[G] Supplemental Figure 3

Howell et al., Supplementary Figure 3

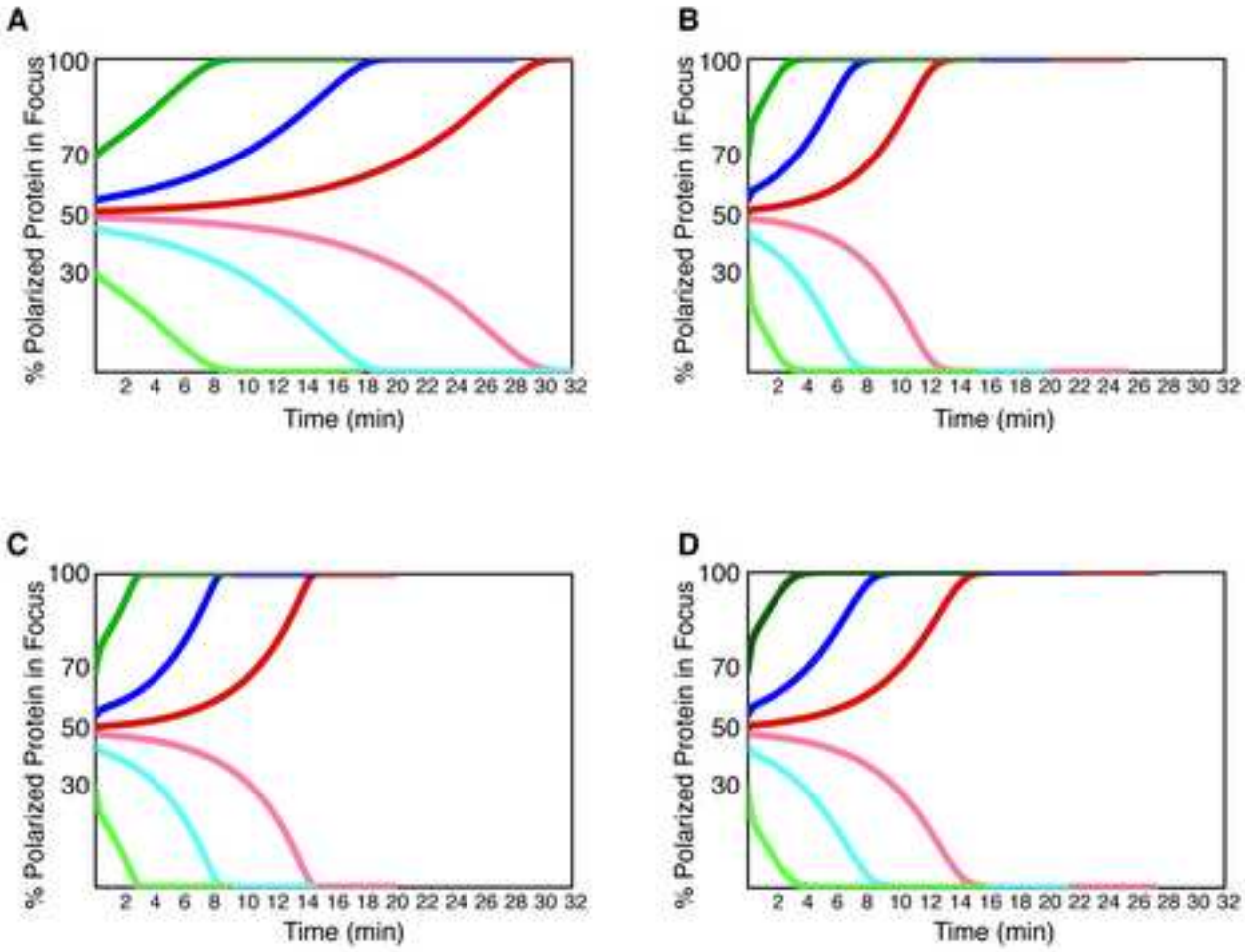

E

Parameter	Key	A	B	C	D
k_1	E_c to E_m	10 s^{-1}	10 s^{-1}	10 s^{-1}	10 s^{-1}
k_{-1}	E_m to E_c	10 s^{-1}	10 s^{-1}	10 s^{-1}	10 s^{-1}
k_2	Basal GEF	0.0001 $\mu M^{-1}s^{-1}$	0.0001 $\mu M^{-1}s^{-1}$	**0.16 $\mu M^{-1}s^{-1}$**	**0.0067 $\mu M^{-1}s^{-1}$**
k_{-2}	GAP	0.017 s^{-1}	0.017 s^{-1}	**0.315 s^{-1}**	**0.016 s^{-1}**
k_3	Stimulated GEF	0.01 $\mu M^{-1}s^{-1}$	0.01 $\mu M^{-1}s^{-1}$	**0.35 $\mu M^{-1}s^{-1}$**	**0.015 $\mu M^{-1}s^{-1}$**
k_4 and k_7	Complex association	10 $\mu M^{-1}s^{-1}$	10 $\mu M^{-1}s^{-1}$	10 $\mu M^{-1}s^{-1}$	10 $\mu M^{-1}s^{-1}$
k_{-4}	Complex dissociation	0.3 s^{-1}	**10 s^{-1}**	**10 s^{-1}**	**10 s^{-1}**
k_5	RDI_c to RDI_m	0.9 s^{-1}	0.9 s^{-1}	0.9 s^{-1}	0.9 s^{-1}
k_{-5}	RDI_m to RDI_c	0.13 s^{-1}	0.13 s^{-1}	0.13 s^{-1}	0.13 s^{-1}
k_6	GDI association	1.5 $\mu M^{-1}s^{-1}$	1.5 $\mu M^{-1}s^{-1}$	1.5 $\mu M^{-1}s^{-1}$	1.5 $\mu M^{-1}s^{-1}$
k_{-6}	GDI dissociation	10 s^{-1}	10 s^{-1}	10 s^{-1}	10 s^{-1}

[G] Supplemental Figure 4

Howell et al., Supplementary Figure 4

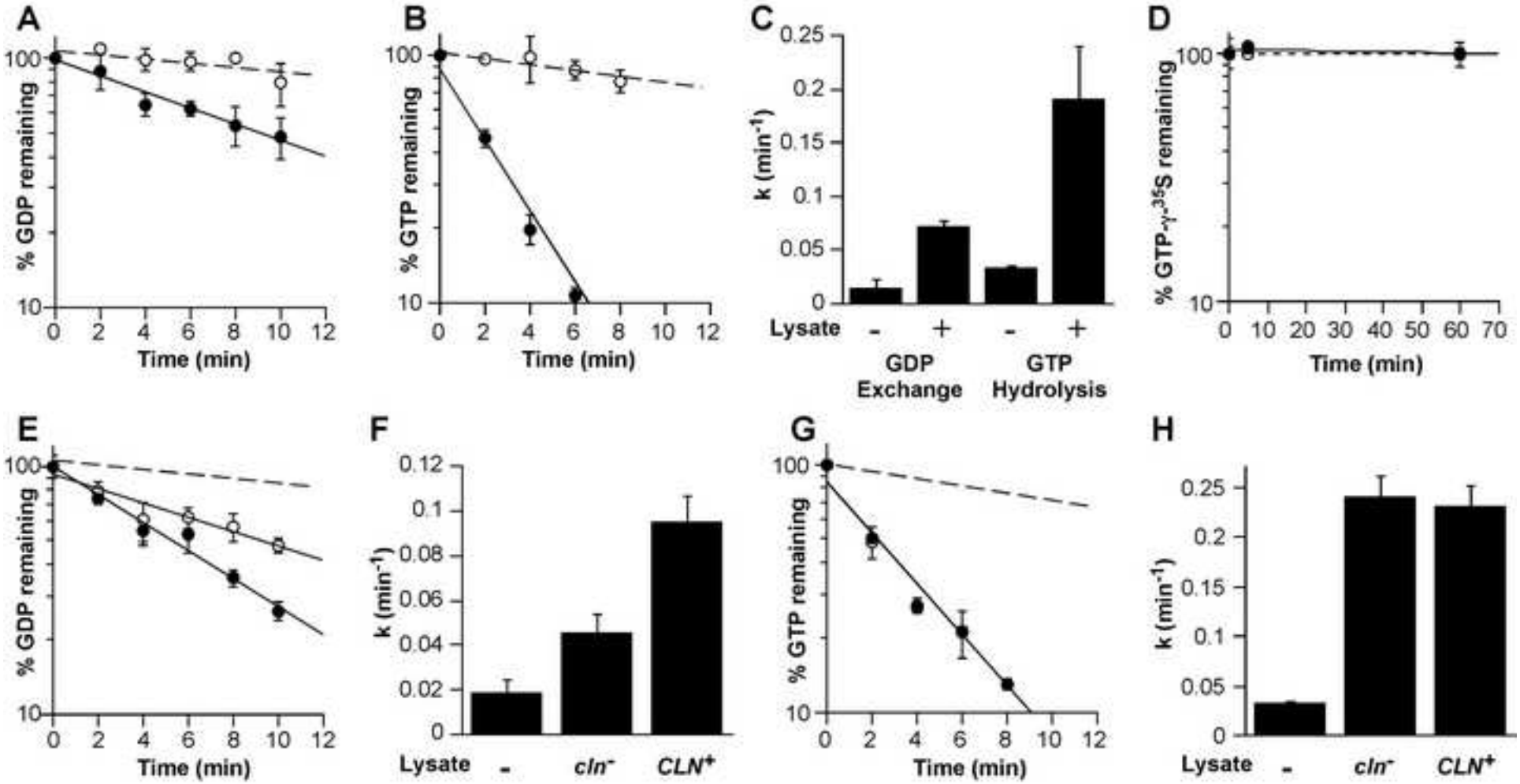

[G] Supplemental Figure 5

Howell et al., Supplementary Figure 5.

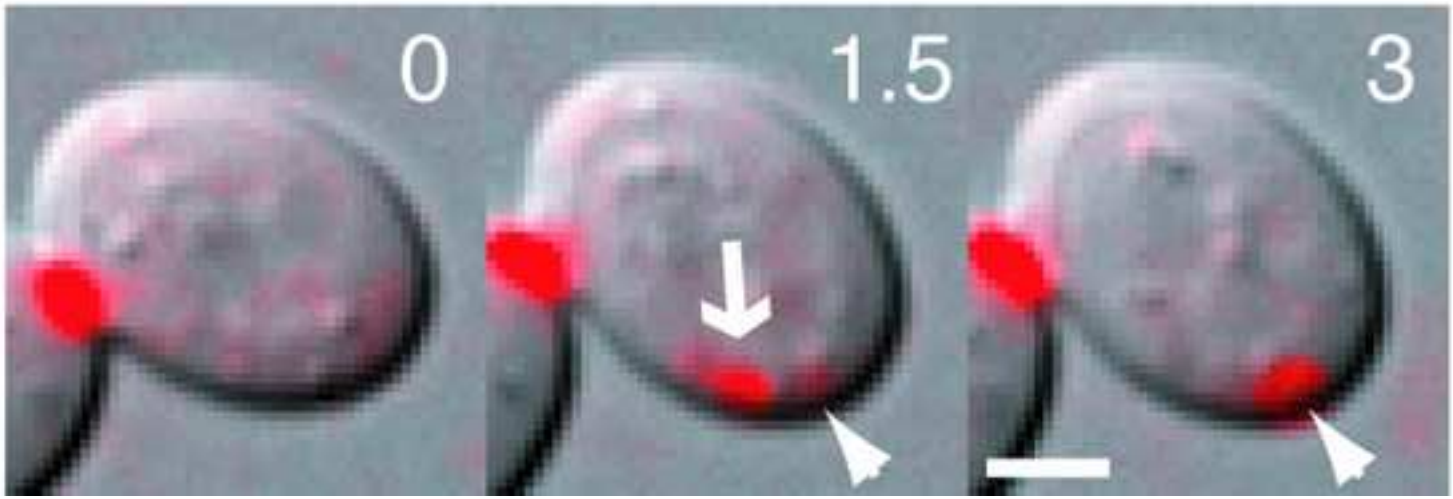

[G] Supplemental Figure 6

Howell et al., Supplementary Figure 6

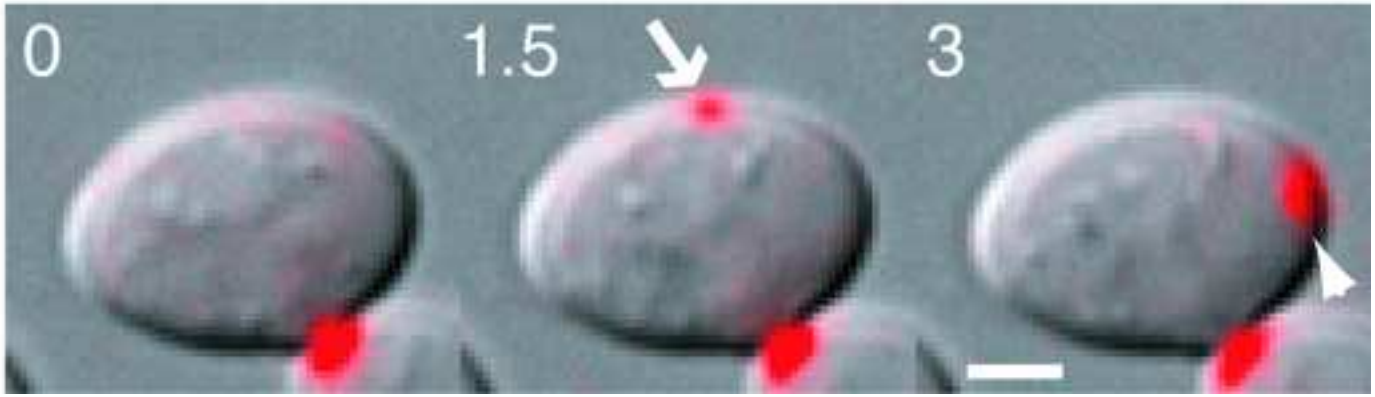

[G] Supplemental Figure 7

Howell et al., Supplementary Figure 7